

# QCD phase diagram in a magnetic field with baryon and isospin chemical potentials

Yu Hamada,<sup>1,2</sup> Muneto Nitta,<sup>3,2,4</sup> and Zebin Qiu<sup>2</sup>

<sup>1</sup>*Deutsches Elektronen-Synchrotron DESY, Notkestr. 85, 22607 Hamburg, Germany*

<sup>2</sup>*Research and Education Center for Natural Sciences, Keio University,*

*4-1-1 Hiyoshi, Yokohama, Kanagawa 223-8521, Japan*

<sup>3</sup>*Department of Physics, Keio University, 4-1-1 Hiyoshi, Yokohama, Kanagawa 223-8521, Japan*

<sup>4</sup>*International Institute for Sustainability with Knotted Chiral Meta Matter(WPI-SKCM<sup>2</sup>), Hiroshima University, 1-3-2 Kagamiyama, Higashi-Hiroshima, Hiroshima 739-8511, Japan*

Based on the chiral perturbation theory at the leading order, we present the phase diagram of low-energy QCD in a magnetic field at finite baryon and isospin chemical potentials. The phase diagram consists of the QCD vacuum, the chiral soliton lattice, the uniform charged pion condensation, an Abrikosov vortex lattice of the charged pions, a baryonic vortex lattice composed of neutral and charged pion vortices with their topological linking number being the baryon number, and a hybrid phase of chiral soliton and vortex lattices, with their intersections carrying the baryon number. While the chiral soliton lattice demands ultra-strong magnetic field  $\sim 10^{19}$  G, the intersection phase appears at  $\sim 10^{17}$  G, which is more realistic in neutron stars.

## INTRODUCTION

Understanding the phase structure of Quantum Chromodynamics (QCD) at finite density remains a fundamental challenge [1–7], due to the nature of strongly correlated systems and the sign problem in lattice QCD. At low energies, chiral perturbation theory (ChPT) [8–12] provides a systematic framework using pion degrees of freedom. Topological effects are encoded in the conserved Goldstone–Wilczek (GW) current [13], which couples baryon number to gauge fields through the Wess–Zumino–Witten (WZW) term [14]. The finite baryon density and electromagnetic (EM) effects are incorporated via  $U(1)_B$  and  $U(1)_{\text{EM}}$  gauge fields [15, 16].

In particular, a magnetic field enriches the QCD phase diagram [17–22], inducing phenomena such as magnetic catalysis (and inverse) [23–25] and inhomogeneous chiral phases [26, 27]. In the hadronic regime, a prominent magnetic phenomenon is the neutral pion  $\pi^0$  domain wall (DW) and its periodic realization, the chiral soliton lattice (CSL) [16, 28, 29]. Through the WZW term, the CSL has lower free energy than the vacuum when the magnetic field exceeds a certain critical value. Such an arising phase carries the baryon number as the topological charge of the GW current [16], suggesting that dense hadronic matter under strong magnetic fields may be dominantly pionic [30]. At higher density and stronger magnetic field, CSL transits to the DW Skyrmiion phase in which Skyrmiions emerge on top of CSL [31–36]. Related studies include  $\eta^{(\prime)}$  CSLs and non-Abelian generalizations [37–41], mixed soliton lattices of  $\pi^0$  and  $\eta^{(\prime)}$  mesons [42], nucleation dynamics of CSLs [43–45] as well as counterparts of CSL in QCD-like, supersymmetric, and holographic theories [46–49] among others [50–52].

Realistic phenomenology also takes into account a finite isospin chemical potential, which triggers the charged pion condensation (CPC) [53–55] and enables lattice simulations free of the sign problem [56–61].

Abrikosov–Nielsen–Olesen (ANO) vortices [62, 63] can exist in such a condensate, and they form an Abrikosov vortex lattice (AVL) in the presence of a magnetic field, which has been studied with either isospin or baryon chemical potential [64–71]. Recently, an ANO-like vortex carrying baryon number, dubbed “baryonic vortex”, has been discovered in the chiral limit [72] or with nonzero pion mass [73]. In the latter case, above a critical baryon chemical potential, a local ANO vortex of charged pions  $\pi^\pm$  becomes topologically linked to a global  $\pi^0$  vortex, with the linking number being the baryon number [74, 75]. The resulting soliton carries the baryon charge homotopic to a Skyrmiion [76–79] or a vortex–Skyrmiion [80–83], whereas realizing a model-independent description of baryons as linked vortices [84].

In this Letter, for the first time, we obtain a three-dimensional phase diagram of low-energy QCD in terms of the magnetic field  $B$ , the baryon chemical potential  $\mu_B$ , and the isospin chemical potentials  $\mu_I$ , see Fig. 1. Our study is performed within leading-order ChPT as a model-independent framework. Augmented with well-defined theoretical approximations, we establish all phase boundaries analytically up to one numerical constant. In addition to established phases such as the QCD vacuum, the CSL, the uniform CPC, and the AVL, our conclusive phase diagram includes a baryonic vortex lattice (BVL), and a CSL–AVL intersection phase. While the CSL requires very strong magnetic fields of order  $10^{19}$  G [16], the CSL–AVL intersection arises at  $10^{17}$  G, thereby opening a new window for anomaly-induced baryonic phase in neutron star interiors at lower magnetic fields than previously expected.

## LEADING ORDER CHIRAL PERTURBATION

We consider low-energy dense baryonic matter under a magnetic field  $B$  at finite baryon chemical potential  $\mu_B$

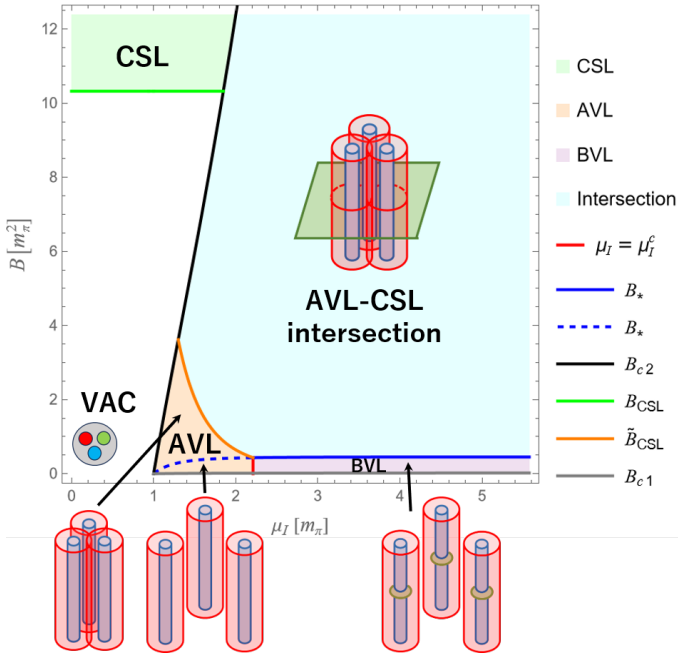


FIG. 1: Phase diagram in one slice of  $(B, \mu_B, \mu_I)$  space at the typical  $\mu_B = 1$  GeV.  $B_{\text{CSL}}$  (green),  $\bar{B}_{\text{CSL}}$  (orange) and  $\mu_I^c$  (red) depend on the value of  $\mu_B$ .  $B_{c1}$  (grey) almost overlaps the horizontal axis because it is far below the scale of this figure. The intersection of the red, blue and orange curves is located at  $\mu_I^c = 307$  MeV and  $B^c = 4.28 \times 10^{17}$  G  $\ll B_{\text{CSL}} = 1.02 \times 10^{19}$  G.

and isospin chemical potential  $\mu_I$ . The dynamics of such a system is effectively described by the ChPT with the WZW term. The chiral Lagrangian for two flavors reads

$$\mathcal{L}_{\text{chiral}} = \frac{f_\pi^2}{4} [\text{Tr} (D^\mu \Sigma^\dagger D_\mu \Sigma) + m_\pi^2 \text{Tr} (\Sigma^\dagger + \Sigma - 2)], \quad (1)$$

where  $\Sigma \in SU(2)$  can be parametrized as

$$\Sigma = \exp(i\boldsymbol{\tau} \cdot \boldsymbol{\pi}) = \begin{pmatrix} \phi_1 & -\phi_2^* \\ \phi_2 & \phi_1^* \end{pmatrix}, \quad |\phi_1|^2 + |\phi_2|^2 = 1, \quad (2)$$

with  $\tau^i$  the Pauli matrices and  $\phi_1$  and  $\phi_2$  complex scalar fields corresponding to the neutral and charged pions, respectively. We fix the pion decay constant  $f_\pi = 93$  MeV and pion mass  $m_\pi = 139$  MeV. The covariant derivative in Eq. (1) is a result of the  $U(1)$  gauging, i.e.,

$$D_\mu \Sigma = \partial_\mu \Sigma - i (e A_\mu + A_\mu^I) [Q, \Sigma], \quad (3)$$

with the charge matrix  $Q = 1/6 + \tau^3/2$  and elementary charge  $e$ . It is worth clarifying that  $A_\mu$  represents the EM gauge field while  $A_\mu^I$  is an effective description to incorporate the isospin chemical potential  $A_\mu^I = (\mu_I, \mathbf{0})$ . Throughout the paper, we consider static configurations with no  $\partial_0$  and consistently, no electric field. To this end, the  $\mu_I$  is set to be a homogeneous input. In our power

counting scheme,<sup>1</sup> the EM Lagrangian is at leading order:

$$\mathcal{L}_{\text{EM}} = \frac{1}{4} F^{\mu\nu} F_{\mu\nu}, \quad F_{\mu\nu} = \partial_\mu A_\nu - \partial_\nu A_\mu. \quad (4)$$

Specifically, we consider a uniform magnetic field along the  $z$ -axis  $\mathbf{B} = B \hat{z}$ .

The magnetic field brings in the effect of the chiral anomaly, which could be captured by the gauged WZW term:

$$\mathcal{L}_{\text{WZW}} = \left( \frac{1}{2} e A_\mu + A_\mu^B \right) j_B^\mu, \quad (5)$$

where  $j_B^\mu$  is the topological GW current

$$j_B = \star \frac{1}{24\pi^2} \text{Tr} \{ l \wedge l \wedge l + 3ieQd [A \wedge (l - r)] \}, \quad (6)$$

with  $l = \Sigma^\dagger d\Sigma$  and  $r = \Sigma d\Sigma^\dagger$ . The charge  $N_B = \int d^3x j_B^0$  has the physical meaning of the baryon number. In parallel to  $A_\mu^I$ , the effective baryon gauge field  $A_\mu^B$  encompasses the baryon chemical potential  $A_\mu^B = (\mu_B, \mathbf{0})$ . Once  $\mu_B$  is introduced, the system tends to accommodate a nonzero  $N_B$  couples to the  $\mu_B$  through the WZW term, reducing the total energy by  $-\mu_B N_B$ .<sup>2</sup> Importantly, a finite  $N_B$  could exist only if neutral pion is involved. There are different solitons that carry the baryon number. One is the DW for which the  $j_B$  originates from the second term in Eq. (6). The associated phase is nothing but the CSL. Another soliton is the Skyrmiion, or technically known as the vortex Skyrmiion in our context given the CPC in the bulk, distinguished from the conventional Skyrmiion. The  $j_B$  of such a soliton is attributed to the  $l \wedge l \wedge l$ -term in Eq. (6), which yields a winding number of the non-trivial homotopy group  $\pi_3(S^3)$ .

## VORTEX AND CHIRAL SOLITON LATTICES

Let us briefly review the effect of finite  $\mu_I$ . For  $\mu_I > m_\pi$  charged pions form the Bose-Einstein condensate, exhibiting superconductivity [55]. Characteristic scales of superconductors are the penetration depth  $\lambda$  and the coherence length  $\xi$  [64] (see Appendix A):

$$\lambda^{-1} = e f_\pi \sqrt{1 - \frac{m_\pi^4}{\mu_I^4}}, \quad \xi^{-1} = \mu_I \sqrt{1 - \frac{m_\pi^4}{\mu_I^4}}, \quad (7)$$

respectively. The Ginzburg-Landau parameter  $\kappa \equiv \lambda/\xi = \mu_I/e f_\pi > m_\pi/e f_\pi \sim 4.93$  with  $e^2/(4\pi) \simeq 1/137$

<sup>1</sup> We adopt the same power counting scheme as Refs. [70, 71], *i.e.*, in terms of the momentum (denoted by  $p$ ) expansion;  $e \sim \mathcal{O}(p^1)$ ,  $A_\mu \sim \mathcal{O}(p^0)$ ,  $\mu_I \sim \mathcal{O}(p^1)$  and  $\mu_B \sim \mathcal{O}(p^{-1})$ .

<sup>2</sup> The first term in Eq. (5) is at subleading  $\mathcal{O}(p^4)$ .

satisfies the condition  $\kappa > 1/\sqrt{2}$  for type-II superconductivity [64, 68]. In parallel to metallic superconductors, there are pionic vortices [64, 65, 68]. Let us explain a single vortex in the cylindrical coordinate  $(\rho, \varphi, z)$ . The dependence on the azimuthal  $\varphi$  of the dynamics is entirely attributed to the charged pion vortex, i.e.,  $\phi_2 = |\phi_2| \exp(i\varphi)$  and  $A = \rho A_\varphi(\rho, z) d\varphi$ . Meanwhile,  $\phi_1$ ,  $\phi_1^*$ ,  $|\phi_2|$  and  $A_\varphi$  remain functions of  $\rho$  and  $z$ , which are to be solved from the equation of motion (EOM) governed by  $\mathcal{L} = \mathcal{L}_{\text{chiral}} + \mathcal{L}_{\text{WZW}} + \mathcal{L}_{\text{EM}}$ , with proper boundary conditions. Whereas details of EOM are omitted since they are identical to those in Ref. [73], the boundary conditions deserve explication, especially on how they conserve the baryon number as a topological charge and why it is so in search of the ground state. There are two kinds of vortices; one is an ANO vortex with no dependence of  $\phi_1$  on  $z$ , which does not carry a baryon number [64, 65, 68]. The other is a baryonic vortex with  $z$ -dependent  $\phi_1$  carrying a baryon number [72, 73]. In either case, each vortex carries a magnetic flux quantum  $\Phi_0 = 2\pi/e$ .

Multiple vortices repel each other and form an AVL in an applied  $B$  among the window  $B_{c1} < B < B_{c2}$  [85]:<sup>3</sup>

$$B_{c1} \equiv \frac{T}{\Phi_0} \sim \frac{ef_\pi^2}{2} \left(1 - \frac{m_\pi^4}{\mu_I^4}\right) \log\left(\frac{\mu_I}{ef\pi}\right), \quad (8)$$

$$B_{c2} \equiv \frac{\Phi_0}{2\pi\xi^2} = \frac{\mu_I^2}{e} \left(1 - \frac{m_\pi^4}{\mu_I^4}\right). \quad (9)$$

Here  $T$  is the tension (energy per unit length) of a vortex and “ $\sim$ ” denotes an order estimation (see Appendix B). The  $B_{c2}$  and  $B_{c1}$  are drawn in Fig. 1 by the black and gray curves respectively. The AVL features the lattice spacing  $a = \sqrt{2/\sqrt{3}n_v}$  with the vortex number density

$$n_v = \frac{B}{\Phi_0} = \frac{eB}{2\pi}. \quad (10)$$

At  $B < B_{c1}$ , vortices do not arise due to the Meissner effect, leaving a uniform CPC. The lattice spacing is  $a \sim \xi$  at  $B = B_{c2}$ , and when  $B > B_{c2}$ , the lattice becomes so dense that superconductivity is broken.

The coexistence of  $\mu_B$  and  $\mu_I$  is essential for the physics we are to illuminate. In the absence of CPC (e.g., at  $B > B_{c2}$ ), the CSL made of pure neutral pion DWs stands as the ground state for  $B$  above [16]

$$B_{\text{CSL}} = \frac{16\pi f_\pi^2 m_\pi}{e\mu_B}, \quad (11)$$

denoted by the green line in Fig. 1.

<sup>3</sup>  $B_{c1}$  can be also written as  $B_{c1} \sim \frac{\Phi_0}{4\pi\lambda^2} \log\left(\frac{\lambda}{\xi}\right)$ .

Region	$B$	$\langle \pi^\pm \rangle$	SC	vortices
$B_{c2} < B$	homogeneous	$= 0$	no	no
$B_{c1} < B < B_{c2}$	inhomogeneous	$\neq 0$	yes	yes
$B < B_{c1}$	homogeneous	$\neq 0$	yes	no

TABLE I: Categorization by the superconductivity or the charged pion condensation at  $\mu_I > m_\pi$ .

### PHASE DIAGRAM IN $(B, \mu_B, \mu_I)$

For clarity, we will present a phase diagram spanned by  $(\mu_I, B)$  at a typical value of  $\mu_B$  plus additional explanation of the dependence on varied  $\mu_B$ . The phases can first be divided into three categories summarized in Table I. First, let us discuss the phases with no vortices.

$B > B_{c2}$ : **QCD vacuum and CSL**. The ground state is CSL when  $B > B_{\text{CSL}}$  is satisfied. Otherwise, it is the QCD vacuum. The  $B_{\text{CSL}}$  is a function of  $\mu_B$  independent of  $\mu_I$ . Hence  $B = B_{\text{CSL}}(\mu_B)$  turns out to be a horizontal line in our phase diagram in Fig. 1. We choose a typical  $\mu_B = 1$  GeV around the nucleon mass to plot the  $B_{\text{CSL}}$ . Such a green line would translate downward (along the  $B$ -axis towards lower  $B$ ) with an increasing  $\mu_B$ , and vice versa. We remark that within the region of “QCD vacuum” there exists the phase of traditional nuclear matter which could be described by a Skyrme crystal [86–88]. Such a description involves the Skyrme term, rendering the results model-dependent. In contrast, our analysis is in the model-independent ChPT. Moreover, within the CSL phase, there are several phase boundaries stipulating the DW Skyrmion phase [31–36] and the charged pion instability [29] etc. They are already established phenomena and not specified in the current work.

$B < B_{c1}$ : **Uniform CPC**. This region could also accommodate the Skyrmion crystal for large  $\mu_B$ , which is not the main focus of the current work.

Now we turn to the phase structure with superconductivity and vortices.

$B_{c1} < B < B_{c2}$  (**Case 1**): **AVL and BVL without CSL**. Three scales are essential; the coherence length  $\xi$ , the penetration depth  $\lambda$ , and the vortex lattice spacing  $a$ . Comparing  $a$  with  $\lambda$  defines a magnetic field  $B_*$

$$a \sim \sqrt{2}\lambda \leftrightarrow B = B_* \equiv c_b \pi e f_\pi^2 \left(1 - \frac{m_\pi^4}{\mu_I^4}\right), \quad (12)$$

with  $c_b$  a constant determined later.  $B_*$  separates

- 1) Dilute  $a \gtrsim \sqrt{2}\lambda \leftrightarrow B_{c1} \lesssim B \lesssim B_*$ ,
- 2) Dense  $\xi < a \lesssim \sqrt{2}\lambda \leftrightarrow B_* \lesssim B \lesssim B_{c2}$

through a crossover. In 1) vortices are well separated. In 2) the magnetic fields of vortices in contiguous cells begin to overlap each other, but vortex cores characterized by

$\xi$  are still distanced from each other. We delineate  $B_*$  with the blue curve in the phase diagram Fig. 1.

In addition to the above classification based on the lattice spacing, the nature of each vortex among a certain lattice can be classified into two cases: an ANO vortex carrying no baryon number versus a baryonic vortex carrying a finite baryon number. The difference is more clearly explained in the dilute regime, where the vortex in one cell does not interfere with others. Whereas the ANO vortex is already described above as the charged pion condensate with a winding phase  $\langle\phi_2\rangle e^{i\varphi}$ , the profile of a baryonic vortex consists in the linking between charged and neutral pions, as detailed in Ref. [73] by the same authors. The phase associated with baryonic vortices, namely BVL, emerges on the condition that  $\mu_I$  is above a critical value as a function of  $\mu_B$ . Otherwise the phase is dominated by the AVL comprised of ANO vortices:

$$\text{a) AVL: } \mu_I < \mu_I^c(\mu_B), \quad \text{b) BVL: } \mu_I > \mu_I^c(\mu_B). \quad (14)$$

The rigorous quantification of  $\mu_I^c$  is established in Ref. [73] numerically. Here alternatively, we present an approximate yet analytical evaluation by imitating the BVL configuration as a simple addition of the neutral pion DW on top of the AVL. The averaged magnetic field sustained by a single ANO vortex within an area bounded by the penetration depth  $\sqrt{2}\lambda$  is:

$$B_{\text{vor}} = c_v \frac{\Phi_0}{(\sqrt{2}\lambda)^2} = c_v \pi e f_\pi^2 \left(1 - \frac{m_\pi^4}{\mu_I^4}\right) \quad (15)$$

with an order-one constant  $c_v$  to be fixed. For the neutral pion DW to emerge inside the ANO string to form a baryonic vortex, such  $B_{\text{vor}}$  surpasses the critical magnetic field of CSL with the modified decay constant

$$\tilde{B}_{\text{CSL}} \equiv \frac{16\pi \tilde{f}_\pi^2 m_\pi}{e\mu_B}; \quad \tilde{f}_\pi \equiv f_\pi |\phi_1| = f_\pi \frac{m_\pi^2}{\mu_I^2}, \quad (16)$$

which applies to regimes with a finite CPC so that  $|\phi_1| \neq 1$ . Then the comparison yields<sup>4</sup>

$$B_{\text{vor}} > \tilde{B}_{\text{CSL}} \leftrightarrow \mu_I > \mu_I^c \equiv m_\pi \sqrt[4]{\frac{16m_\pi}{c_v e^2 \mu_B}} + 1. \quad (17)$$

We find this approximation quite good when fitting with numerical results which leads to  $c_v = 1.06$  as detailed in Appendix C.<sup>5</sup> We plot the  $\mu_I^c(\mu_B = 1 \text{ GeV})$  on the

phase diagram in Fig. 1 with the red line. The transition between AVL and BVL starts inside the individual vortex, and the magnetic field affects only the lattice spacing  $a$  but not an internal structure of each vortex, as far as vortices are well separated,  $B < B_*$ . Therefore,  $\mu_I^c$  itself does not depend on  $B$ , yielding a vertical line. Such a vertical line would translate leftwards (along the  $\mu_I$ -axis towards smaller  $\mu_I$ ), when  $\mu_B$  increases, in view of Eq. (17). In the limit  $\mu_B \rightarrow \infty$ ,  $\mu_I^c = m_\pi$  implies that the only possible vortex lattice phase is BVL. Conversely, for  $\mu_B \rightarrow 0$ , the infinite  $\mu_I^c \rightarrow \infty$  indicates that BVL cannot emerge. These limiting behaviors are exhibited in Appendix D.

The configuration of dense BVL around  $B = B_*$  will be altered, different from a simple assemblage of well-separated baryonic vortices which were profiled in Ref. [73]. The specific solution should be attained under carefully tailored boundary conditions, including the inter-vortex interactions, which is reserved for future work.

Combining two ways of classification, we summarize that phases of vortex lattices fall into four categories: 1a) dilute AVL, 1b) dense AVL, 2a) dilute BVL, and 2b) dense BVL. We will show that 2b) does not happen.

$B_{c1} < B < B_{c2}$  (**Case 2: AVL-CSL intersection**). A necessary condition for a CSL to appear in phases with vortices is  $B > \tilde{B}_{\text{CSL}}$  with noticing the modified  $\tilde{f}_\pi$  in Eq. (16). This condition is valid as long as  $B < B_{c2}$ . In such a range,  $\tilde{B}_{\text{CSL}}$  is plotted by the orange curve in Fig. 1. Although the CSL can be stable when the magnetic field is uniform, it is not the case if the magnetic field is localized by vortices: a chiral soliton will decay in the inter-vortex region outside penetration depth  $\lambda$ , where the magnetic field is absent when vortices are well separated  $a \gg \lambda$ . Thus, the curve  $B = \tilde{B}_{\text{CSL}}$  is invalid below  $B < B_*$ . Such a decay of chiral solitons is avoided in denser vortex lattices with  $B > B_*$  where the lattice spacing is smaller than the penetration depth so the magnetic fields of contiguous vortices overlap each other. As a result, despite the vortices, the overall magnetic field is nearly uniform, supporting the CSL. Then here is the condition for CSL to coexist with AVL and form intersections:

$$\max(\tilde{B}_{\text{CSL}}, B_*) < B < B_{c2}. \quad (18)$$

Let us take a closer look at what happens on the phase boundary  $B_*$ . In BVL, each baryonic vortex penetrates a pancake-shaped chiral soliton whose edge is a closed  $\pi_0$  string (in the  $x$ - $y$  plane).<sup>6</sup> The pancakes of contiguous

<sup>4</sup> In this approximation, we have ignored the tension of a neutral pion vortex attached to the chiral soliton (see Appendix B).

<sup>5</sup> We use data with  $\mu_I \geq 3.5m_\pi$  for fitting since the numerical solutions of the baryonic vortices could not be found for  $\mu_I \lesssim 3.5m_\pi$  within  $\mathcal{O}(p^2)$  ChPT. However, even with that regime, we expect that  $\mathcal{O}(p^4)$  ChPT with the so-called Skyrme term exhibits stable baryonic vortices and that Eq. (17) still holds within certain accuracy.

<sup>6</sup> The radius of the pancakes is typically the same as  $\xi \sim 1/\mu_I \sim 0.13/f_\pi$  for  $\mu_I \sim 5m_\pi$ , so that ChPT based on the expansion with respect to  $|p| \ll 4\pi f_\pi \sim f_\pi/0.08$  is still marginally valid. One should note that the current ChPT breaks down at  $\mu_I \sim 5.6m_\pi$  where  $\rho$  meson must be taken into account.

baryonic vortices attract each other because the nearest points between two neighbored  $\pi^0$  strings have opposite windings, and thus they sit in the same position along the vortices. When the magnetic field  $B$  is larger than the phase boundary  $B_*$ , the AVL-CSL intersection is energetically favored, which can be regarded as a configuration after the pancakes enlarge transversely and attach each other to form an infinitely large  $\pi_0$  DW. On the other hand,  $B = B_*$  does not prescribe a phase boundary within the AVL phase (see the dotted segment of the blue curve). What separates the phases of AVL and AVL-CSL intersection is  $B = \tilde{B}_{\text{CSL}}$ , at which the transition is not associated with such a deformation of chiral solitons, unlike that of BVL.

Finally, we elaborate why the orange, blue, and red curves should intersect at one triple point, which is achieved by  $c_b = c_v$ . When a state with vortices is adiabatically changed across the blue curve  $B = B_*$ , only the inter-vortex distance is altered while the strength of the magnetic field inside a vortex is unchanged, so a chiral soliton can not be created or annihilated during such a process. Thereby, the blue curve could neither separate AVL from BVL, nor AVL from CSL-CSL intersection. Then in Fig. 1, the three curves,  $B = \tilde{B}_{\text{CSL}}$ ,  $B = B_*$  and  $\mu_I = \mu_I^c$ , must join at a common intersection at

$$(\mu_I^c, B^c) = \left( m_\pi \sqrt[4]{\frac{16m_\pi}{c_v e^2 \mu_B} + 1}, \frac{c_v \pi e f_\pi^2}{1 + \frac{c_v e^2 \mu_B}{16m_\pi}} \right). \quad (19)$$

For  $\mu_B = 1$  GeV, we have  $\mu_I^c = 307$  MeV and  $B^c = 4.28 \times 10^{17}$  G whereas  $B_{\text{CSL}} = 1.02 \times 10^{19}$  G (see Appendix D).

### Baryon number densities.

Among the phases in Fig. 1, CSL, BVL, and AVL-CSL intersection carry baryon numbers. They have different profiles but the same averaged area density (in the  $x$ - $y$  plane) of the baryon number. The area density of a single soliton in the CSL is homogeneously  $eB/2\pi$  [16]. In comparison, for the AVL-CSL intersection phase, it is

$$\int_0^{2\pi} dz \partial_z \pi_0 \frac{e}{4\pi^2} \int d^2x F_{12} = \frac{e}{2\pi} \Phi_0 \langle n_v \rangle = \frac{e \langle B \rangle}{2\pi} \quad (20)$$

with the vortex number density  $n_v$  defined in Eq. (10). The only difference from the CSL is that the magnetic field is not uniform. However, the averaged magnetic fields are equal, so is the density. The baryon numbers of CSL and CSL-CSL intersection both come from the term  $\propto d[A \wedge (l - r)]$  in Eq. (6). Instead, in the BVL, each baryonic vortex carries  $N_B = 1$  contributed from the  $l \wedge l \wedge l$ -term as the linking number of the ANO vortex and  $\pi_0$  vortex [73]. From Eq. (10), the baryon number density within one period (along the  $z$ -axis) is

$$N_B n_v = \frac{e \langle B \rangle}{2\pi}. \quad (21)$$

The coincidence of the baryon densities in these three phases is not accidental, but reflects the topologically protected anomaly nature across distinct phases.

### SUMMARY

We presented the phase diagram in Fig. 1 of low-energy QCD in a magnetic field at finite baryon and isospin chemical potentials in leading-order ChPT. The baryonic vortex proposed as topologically linked neutral and charged pion vortices constitutes a phase called BVL, which is induced by a finite  $\mu_B$  on top of an AVL, occupying the region with higher  $\mu_I$  on the phase diagram. Also revealed is a phase of AVL-CSL intersection which borders vacuum, CSL, AVL, and BVL, dominating the large  $B$  regime. Within a legitimate approximation, all phase boundaries are obtained analytically, except for one numerical constant. The baryon number densities of CSL, BVL, and AVL-CSL were shown to coincide, reflecting their common anomaly-induced topological origin.

The characteristic magnetic field in the current study typified by  $B^c \sim 10^{17}$  G applies to the context of heavy-ion collisions. However, the  $\mu_I^c \sim 300$  MeV is rather large compared to the typical  $\mu_I \lesssim 10$  MeV. Nonetheless, neutron stars typically feature  $\mu_I \sim 50$ –150 MeV, with the possibility to reach  $\mu_I \sim 200$ –300 MeV in the cores. In the same context,  $\mu_B \sim 1$ –2 GeV and strong magnetic fields  $B \sim 10^{16}$ – $10^{18}$  G can exist. These facts suggest the prominent relevance of the AVL-CSL intersection and BVL in the core of neutron stars. In such a regime, various exotic phases come into play, e.g., pion condensed, hyperonic, and Fulde–Ferrell–Larkin–Ovchinnikov phases [55]. Understanding their competition in the phase diagram remains a future task.

**Acknowledgments.** We thank Naoki Yamamoto and Geraint W. Evans for useful comments. This work is supported in part by JSPS Grant-in-Aid for Scientific Research KAKENHI Grant No. JP22H01221 and JP23K22492 (M. N. and Z. Q.) and by the Deutsche Forschungsgemeinschaft under Germany’s Excellence Strategy - EXC 2121 Quantum Universe - 390833306. The work of M. N. is supported in part by the WPI program “Sustainability with Knotted Chiral Meta Matter (WPI-SKCM<sup>2</sup>)” at Hiroshima University.

---

- [1] G. Eichmann, H. Sanchis-Alepuz, R. Williams, R. Alkofer and C. S. Fischer, *Baryons as relativistic three-quark bound states*, *Prog. Part. Nucl. Phys.* **91** (2016) 1 [[1606.09602](#)].
- [2] C. Schmidt and S. Sharma, *The phase structure of QCD*, *J. Phys. G* **44** (2017) 104002 [[1701.04707](#)].
- [3] C. S. Fischer, *QCD at finite temperature and chemical potential from Dyson–Schwinger equations*, *Prog. Part. Nucl. Phys.* **105** (2019) 1 [[1810.12938](#)].
- [4] A. Rothkopf, *Heavy Quarkonium in Extreme Conditions*, *Phys. Rept.* **858** (2020) 1 [[1912.02253](#)].
- [5] J. N. Guenther, *Overview of the QCD phase diagram*:

Recent progress from the lattice, *Eur. Phys. J. A* **57** (2021) 136 [[2010.15503](#)].

[6] V. V. Braguta, *Phase Diagram of Dense Two-Color QCD at Low Temperatures*, *Symmetry* **15** (2023) 1466.

[7] C. Adam, A. Garcia Martin-Caro, M. Huidobro and A. Wereszczynski, *Skyrme Crystals, Nuclear Matter and Compact Stars*, *Symmetry* **15** (2023) 899 [[2305.06639](#)].

[8] J. W. Holt, M. Rho and W. Weise, *Chiral symmetry and effective field theories for hadronic, nuclear and stellar matter*, *Phys. Rept.* **621** (2016) 2 [[1411.6681](#)].

[9] H. W. Hammer, S. König and U. van Kolck, *Nuclear effective field theory: status and perspectives*, *Rev. Mod. Phys.* **92** (2020) 025004 [[1906.12122](#)].

[10] C. Drischler, J. W. Holt and C. Wellenhofer, *Chiral Effective Field Theory and the High-Density Nuclear Equation of State*, *Ann. Rev. Nucl. Part. Sci.* **71** (2021) 403 [[2101.01709](#)].

[11] J. Gasser and H. Leutwyler, *Chiral Perturbation Theory to One Loop*, *Annals Phys.* **158** (1984) 142.

[12] S. Scherer, *Introduction to chiral perturbation theory*, *Adv. Nucl. Phys.* **27** (2003) 277 [[hep-ph/0210398](#)].

[13] J. Goldstone and F. Wilczek, *Fractional Quantum Numbers on Solitons*, *Phys. Rev. Lett.* **47** (1981) 986.

[14] E. Witten, *Global Aspects of Current Algebra*, *Nucl. Phys. B* **223** (1983) 422.

[15] D. T. Son and A. R. Zhitnitsky, *Quantum anomalies in dense matter*, *Phys. Rev. D* **70** (2004) 074018 [[hep-ph/0405216](#)].

[16] D. T. Son and M. A. Stephanov, *Axial anomaly and magnetism of nuclear and quark matter*, *Phys. Rev. D* **77** (2008) 014021 [[0710.1084](#)].

[17] D. E. Kharzeev, *Topology, magnetic field, and strongly interacting matter*, *Ann. Rev. Nucl. Part. Sci.* **65** (2015) 193 [[1501.01336](#)].

[18] V. A. Miransky and I. A. Shovkovy, *Quantum field theory in a magnetic field: From quantum chromodynamics to graphene and Dirac semimetals*, *Phys. Rept.* **576** (2015) 1 [[1503.00732](#)].

[19] J. O. Andersen, W. R. Naylor and A. Tranberg, *Phase diagram of QCD in a magnetic field: A review*, *Rev. Mod. Phys.* **88** (2016) 025001 [[1411.7176](#)].

[20] A. Yamamoto, *Overview of external electromagnetism and rotation in lattice QCD*, *Eur. Phys. J. A* **57** (2021) 211 [[2103.00237](#)].

[21] G. Cao, *Recent progresses on QCD phases in a strong magnetic field: views from Nambu–Jona–Lasinio model*, *Eur. Phys. J. A* **57** (2021) 264 [[2103.00456](#)].

[22] S. Iwasaki, M. Oka and K. Suzuki, *A review of quarkonia under strong magnetic fields*, *Eur. Phys. J. A* **57** (2021) 222 [[2104.13990](#)].

[23] K. G. Klimenko, *Three-dimensional Gross–Neveu model in an external magnetic field*, *Teor. Mat. Fiz.* **89** (1991) 211.

[24] F. Bruckmann, G. Endrodi and T. G. Kovacs, *Inverse magnetic catalysis and the Polyakov loop*, *JHEP* **04** (2013) 112 [[1303.3972](#)].

[25] Y. Aoki, G. Endrodi, Z. Fodor, S. D. Katz and K. K. Szabo, *The Order of the quantum chromodynamics transition predicted by the standard model of particle physics*, *Nature* **443** (2006) 675 [[hep-lat/0611014](#)].

[26] G. Basar, G. V. Dunne and D. E. Kharzeev, *Chiral Magnetic Spiral*, *Phys. Rev. Lett.* **104** (2010) 232301 [[1003.3464](#)].

[27] E. Nakano and T. Tatsumi, *Chiral symmetry and density wave in quark matter*, *Phys. Rev. D* **71** (2005) 114006 [[hep-ph/0411350](#)].

[28] M. Eto, K. Hashimoto and T. Hatsuda, *Ferromagnetic neutron stars: axial anomaly, dense neutron matter, and pionic wall*, *Phys. Rev. D* **88** (2013) 081701 [[1209.4814](#)].

[29] T. Brauner and N. Yamamoto, *Chiral Soliton Lattice and Charged Pion Condensation in Strong Magnetic Fields*, *JHEP* **04** (2017) 132 [[1609.05213](#)].

[30] T. Brauner, *Dense matter in strong magnetic fields without nucleons*, *PoS Confinement2018* (2018) 201.

[31] M. Eto, K. Nishimura and M. Nitta, *Domain-Wall Skyrmion Phase in Dense QCD at Strong Magnetic Fields Using Leading-Order Chiral Perturbation Theory*, *Phys. Rev. Lett.* **134** (2025) 181902 [[2304.02940](#)].

[32] M. Eto, K. Nishimura and M. Nitta, *Phase diagram of QCD matter with magnetic field: domain-wall Skyrmion chain in chiral soliton lattice*, *JHEP* **12** (2023) 032 [[2311.01112](#)].

[33] Y. Amari, M. Eto and M. Nitta, *Domain-wall Skyrmion phase of QCD in magnetic field: gauge field dynamics*, *JHEP* **05** (2025) 037 [[2409.08841](#)].

[34] M. Eto, K. Nishimura and M. Nitta, *Domain-wall Skyrmion phase in a rapidly rotating QCD matter*, *JHEP* **01** (2024) 019 [[2310.17511](#)].

[35] Y. Amari, M. Nitta and R. Yokokura, *Spin statistics and surgeries of topological solitons in QCD matter in magnetic field*, *JHEP* **02** (2025) 171 [[2406.14419](#)].

[36] P. Copinger, M. Eto, M. Nitta and Z. Qiu, *Fermionic domain-wall Skyrmions of QCD in a magnetic field*, [2512.22023](#).

[37] X.-G. Huang, K. Nishimura and N. Yamamoto, *Anomalous effects of dense matter under rotation*, *JHEP* **02** (2018) 069 [[1711.02190](#)].

[38] K. Nishimura and N. Yamamoto, *Topological term, QCD anomaly, and the  $\eta'$  chiral soliton lattice in rotating baryonic matter*, *JHEP* **07** (2020) 196 [[2003.13945](#)].

[39] H.-L. Chen, X.-G. Huang and J. Liao, *QCD phase structure under rotation*, *Lect. Notes Phys.* **987** (2021) 349 [[2108.00586](#)].

[40] M. Eto, K. Nishimura and M. Nitta, *Phases of rotating baryonic matter: non-Abelian chiral soliton lattices, antiferro-isospin chains, and ferri/ferromagnetic magnetization*, *JHEP* **08** (2022) 305 [[2112.01381](#)].

[41] M. Eto, K. Nishimura and M. Nitta, *Non-Abelian chiral soliton lattice in rotating QCD matter: Nambu–Goldstone and excited modes*, *JHEP* **03** (2024) 035 [[2312.10927](#)].

[42] Z. Qiu and M. Nitta, *Quasicrystals in QCD*, *JHEP* **05** (2023) 170 [[2304.05089](#)].

[43] M. Eto and M. Nitta, *Quantum nucleation of topological solitons*, *JHEP* **09** (2022) 077 [[2207.00211](#)].

[44] T. Higaki, K. Kamada and K. Nishimura, *Formation of a chiral soliton lattice*, *Phys. Rev. D* **106** (2022) 096022 [[2207.00212](#)].

[45] M. Eto, K. Nishimura and M. Nitta, *Dislocations and crystallization dynamics of chiral soliton lattices*, [2506.16354](#).

[46] T. Brauner, G. Filios and H. Kolešová, *Anomaly-Induced Inhomogeneous Phase in Quark Matter without the Sign Problem*, *Phys. Rev. Lett.* **123** (2019) 012001 [[1902.07522](#)].

[47] T. Brauner, G. Filios and H. Kolešová, *Chiral soliton lattice in QCD-like theories*, *JHEP* **12** (2019) 029 [[1905.11409](#)].

[48] M. Nitta and S. Sasaki, *Solitonic ground state in supersymmetric theory in background*, *JHEP* **10** (2024) 178 [[2404.12066](#)].

[49] M. A. G. Amano, M. Eto, M. Nitta and S. Sasaki, *Holographic QCD Matter: Chiral Soliton Lattices in Strong Magnetic Field*, *JHEP* (2025) [[2507.16897](#)].

[50] A. Yamada and N. Yamamoto, *Floquet vacuum engineering: Laser-driven chiral soliton lattice in the QCD vacuum*, *Phys. Rev. D* **104** (2021) 054041 [[2107.07074](#)].

[51] T. Brauner and H. Kolešová, *Chiral soliton lattice at next-to-leading order*, *JHEP* **07** (2023) 163 [[2302.06902](#)].

[52] F. Canfora, N. Grandi, M. Lagos, L. Urrutia-Reyes and A. Vera, *Universality of the chiral soliton lattice in the low energy limit of QCD*, [2510.11946](#).

[53] V. Ruck, M. Gyulassy and W. Greiner, *Pion Condensation in Heavy Ion Collisions*, *Z. Phys. A* **277** (1976) 391.

[54] A. B. Migdal, *Pion Fields in Nuclear Matter*, *Rev. Mod. Phys.* **50** (1978) 107.

[55] D. T. Son and M. A. Stephanov, *QCD at finite isospin density*, *Phys. Rev. Lett.* **86** (2001) 592 [[hep-ph/0005225](#)].

[56] J. B. Kogut and D. K. Sinclair, *Quenched lattice QCD at finite isospin density and related theories*, *Phys. Rev. D* **66** (2002) 014508 [[hep-lat/0201017](#)].

[57] J. B. Kogut and D. K. Sinclair, *Lattice QCD at finite isospin density at zero and finite temperature*, *Phys. Rev. D* **66** (2002) 034505 [[hep-lat/0202028](#)].

[58] J. B. Kogut and D. K. Sinclair, *The Finite temperature transition for 2-flavor lattice QCD at finite isospin density*, *Phys. Rev. D* **70** (2004) 094501 [[hep-lat/0407027](#)].

[59] B. B. Brandt, G. Endrodi and S. Schmalzbauer, *QCD phase diagram for nonzero isospin-asymmetry*, *Phys. Rev. D* **97** (2018) 054514 [[1712.08190](#)].

[60] B. B. Brandt, F. Cuteri and G. Endrodi, *Equation of state and speed of sound of isospin-asymmetric QCD on the lattice*, *JHEP* **07** (2023) 055 [[2212.14016](#)].

[61] NPLQCD collaboration, *Lattice quantum chromodynamics at large isospin density*, *Phys. Rev. D* **108** (2023) 114506 [[2307.15014](#)].

[62] A. A. Abrikosov, *On the Magnetic properties of superconductors of the second group*, *Sov. Phys. JETP* **5** (1957) 1174.

[63] H. B. Nielsen and P. Olesen, *Vortex Line Models for Dual Strings*, *Nucl. Phys. B* **61** (1973) 45.

[64] P. Adhikari, T. D. Cohen and J. Sakowitz, *Finite Isospin Chiral Perturbation Theory in a Magnetic Field*, *Phys. Rev. C* **91** (2015) 045202 [[1501.02737](#)].

[65] P. Adhikari, *Magnetic Vortex Lattices in Finite Isospin Chiral Perturbation Theory*, *Phys. Lett. B* **790** (2019) 211 [[1810.03663](#)].

[66] F. Canfora, S. Carignano, M. Lagos, M. Mannarelli and A. Vera, *Pion crystals hosting topologically stable baryons*, *Phys. Rev. D* **103** (2021) 076003 [[2012.05921](#)].

[67] P. Adhikari, E. Leeser and J. Markowski, *Phonon modes of magnetic vortex lattices in finite isospin chiral perturbation theory*, *Mod. Phys. Lett. A* **38** (2023) 2350078 [[2205.13369](#)].

[68] M. S. Grønli and T. Brauner, *Competition of chiral soliton lattice and Abrikosov vortex lattice in QCD with isospin chemical potential*, *Eur. Phys. J. C* **82** (2022) 354 [[2201.07065](#)].

[69] F. Canfora, M. Lagos and A. Vera, *Superconducting multi-vortices and a novel BPS bound in chiral perturbation theory*, *JHEP* **10** (2024) 224 [[2405.08082](#)].

[70] G. W. Evans and A. Schmitt, *Chiral anomaly induces superconducting baryon crystal*, *JHEP* **09** (2022) 192 [[2206.01227](#)].

[71] G. W. Evans and A. Schmitt, *Chiral Soliton Lattice turns into 3D crystal*, *JHEP* **2024** (2024) 041 [[2311.03880](#)].

[72] Z. Qiu and M. Nitta, *Baryonic vortex phase and magnetic field generation in QCD with isospin and baryon chemical potentials*, *JHEP* **06** (2024) 139 [[2403.07433](#)].

[73] Y. Hamada, M. Nitta and Z. Qiu, *Baryons as linked vortices in QCD matter with isospin asymmetry*, *JHEP* (2025) [[2509.20844](#)].

[74] S. B. Gudnason and M. Nitta, *Linking number of vortices as baryon number*, *Phys. Rev. D* **101** (2020) 065011 [[2002.01762](#)].

[75] S. B. Gudnason and M. Nitta, *Linked vortices as baryons in the miscible BEC-Skyrme model*, *Phys. Rev. D* **102** (2020) 045022 [[2006.04067](#)].

[76] T. H. R. Skyrme, *A Nonlinear field theory*, *Proc. Roy. Soc. Lond. A* **260** (1961) 127.

[77] G. S. Adkins, C. R. Nappi and E. Witten, *Static Properties of Nucleons in the Skyrme Model*, *Nucl. Phys. B* **228** (1983) 552.

[78] G. S. Adkins and C. R. Nappi, *The Skyrme Model with Pion Masses*, *Nucl. Phys. B* **233** (1984) 109.

[79] I. Zahed and G. E. Brown, *The Skyrme Model*, *Phys. Rept.* **142** (1986) 1.

[80] S. B. Gudnason and M. Nitta, *Incarnations of Skyrmions*, *Phys. Rev. D* **90** (2014) 085007 [[1407.7210](#)].

[81] S. B. Gudnason and M. Nitta, *Baryonic torii: Toroidal baryons in a generalized Skyrme model*, *Phys. Rev. D* **91** (2015) 045027 [[1410.8407](#)].

[82] S. B. Gudnason and M. Nitta, *Skyrmions confined as beads on a vortex ring*, *Phys. Rev. D* **94** (2016) 025008 [[1606.00336](#)].

[83] M. Nitta, *Fractional instantons and bions in the principal chiral model on  $\mathbb{R}^2 \times S^1$  with twisted boundary conditions*, *JHEP* **08** (2015) 063 [[1503.06336](#)].

[84] M. Eto, Y. Hamada and M. Nitta, *Tying knots in particle physics*, *Phys. Rev. Lett.* **135** (2025) 091603 [[2407.11731](#)].

[85] M. Tinkham, *Introduction to Superconductivity*. Dover Publications, Mineola, NY, 2004.

[86] I. R. Klebanov, *Nuclear Matter in the Skyrme Model*, *Nucl. Phys. B* **262** (1985) 133.

[87] S. Chen, K. Fukushima and Z. Qiu, *Skyrmions in a magnetic field and  $\pi/0$  domain wall formation in dense nuclear matter*, *Phys. Rev. D* **105** (2022) L011502 [[2104.11482](#)].

[88] Y. Amari, M. Nitta and Z. Qiu, *Phase boundary of nuclear matter in magnetic field*, *JHEP* **10** (2025) 180 [[2504.08379](#)].

## End Matter

### Appendix A: Characteristic Lengths

We derive the effective theory for the Higgs mode and obtain the coherence length. For simplicity, we turn down the gauge field and reduce the Hamiltonian to

$$\mathcal{H}_{\text{chiral}} = \frac{f_\pi^2}{2} \left\{ |\nabla \phi_1|^2 + |\nabla \phi_2|^2 - \mu_I^2 |\phi_2|^2 + m_\pi^2 (2 - \phi_1 - \phi_1^*) \right\}. \quad (22)$$

The coherence length  $\xi$  is proportional to the inverse of the effective Higgs mass, which is inferred from the expansion of  $\phi_2$  around its vacuum expectation value:

$$|\phi_2| = \sqrt{1 - m_\pi^4/\mu_I^4} + \delta, \quad \phi_1 = \sqrt{1 - \left( \sqrt{1 - m_\pi^4/\mu_I^4} + \delta \right)^2}. \quad (23)$$

We expand Eq. (22) up to  $\mathcal{O}(\delta^2)$ , attaining the effective Hamiltonian density for the Higgs mode as

$$\mathcal{H}_\delta = \frac{f_\pi^2 \mu_I^4}{2m_\pi^4} [(\nabla \delta)^2 + \xi^{-2} \delta^2], \quad (24)$$

with  $\xi$  the coherence length:<sup>7</sup>

$$\xi^{-2} = \mu_I^2 \left( 1 - \frac{m_\pi^4}{\mu_I^4} \right). \quad (25)$$

On the other hand, the penetration depth  $\lambda$  is proportional to the inverse mass of  $A_\mu$ , which can be read off from the mass term in the form of  $m_A^2 A_\mu A^\mu/2$  among Eq. (1) after expansion near the uniform ground state:

$$\lambda^{-2} = m_A^2 = e^2 f_\pi^2 |\phi_2|^2 = e^2 f_\pi^2 \left( 1 - \frac{m_\pi^4}{\mu_I^4} \right). \quad (26)$$

### Appendix B: Vortex tension

We evaluate the string tensions *i.e.*, the energies per unit length, of an ANO (charged pion) vortex and a neutral pion vortex. The former can be calculated as

$$\begin{aligned} T &\simeq \int d^2x \left[ \frac{f_\pi^2}{2} \left( |\nabla[|\phi_2| \exp(i\varphi)]|^2 + |\nabla|\phi_1||^2 \right) + \frac{1}{2} B^2 \right] \\ &\simeq \frac{f_\pi^2}{2} \left( 1 - \frac{m_\pi^4}{\mu_I^4} \right) \int_0^{2\pi} d\varphi \int_\xi^\lambda \frac{d\rho}{\rho} + c, \\ &= \pi f_\pi^2 \left( 1 - \frac{m_\pi^4}{\mu_I^4} \right) \log \left( \frac{\mu_I}{e f_\pi} \right) + c, \end{aligned} \quad (27)$$

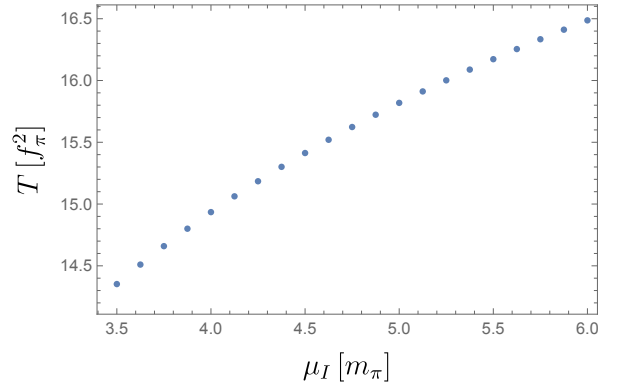


FIG. 2: ANO vortex tension by numerical calculations.

where we have used the facts that the vortex behaves as a global vortex inside the penetration depth  $\rho \lesssim \lambda$  and  $|\phi_2| \sim 1 - \frac{m_\pi^4}{\mu_I^4}$  at  $\rho \gtrsim \xi$ . Here,  $c$  includes several contributions: the gradient energies of  $\phi_{1,2}$  inside the coherence length  $\rho \lesssim \xi$ , an energy of the magnetic field, and the negligible (exponentially suppressed) contributions outside  $\rho \gtrsim \lambda$ . For  $\mu_I/m_\pi = 4.0$ , the first term in Eq. (27) is analytically computed  $\sim 10 f_\pi^2$ , compared to the numerically obtained  $T \sim 15 f_\pi^2$  (see Fig. 2), indicating that Eq. (27) gives a good order estimation with  $c \sim \mathcal{O}(1)$ . The  $c$  in the evaluation of  $B_{c1}$  has been ignored in Fig. 1 because  $B_{c1}$  is much smaller than other scales regardless of  $c$ .

The string tension of a neutral pion vortex attached to the boundary of a chiral soliton can be estimated as

$$\begin{aligned} T_{\pi_0} &\simeq \int d^2x \left[ \frac{f_\pi^2}{2} \left( |\nabla[|\phi_1| \exp(i\varphi)]|^2 + |\nabla|\phi_2||^2 \right) \right] \\ &\simeq \frac{f_\pi^2 m_\pi^4}{2 \mu_I^4} \int_0^{2\pi} d\varphi \int_\xi^{m_\pi^{-1}} \frac{d\rho}{\rho} + b, \\ &= \frac{\pi \tilde{f}_\pi^2}{2} \log \left[ \frac{\mu_I^2}{m_\pi^2} \left( 1 - \frac{m_\pi^4}{\mu_I^4} \right) \right] + b, \end{aligned} \quad (28)$$

where the vortex exists within the core size  $m_\pi^{-1}$  of the chiral soliton, and it becomes vacuum outside.  $b$  is a contribution inside  $\xi$ .  $T_{\pi_0}$  is parametrically small compared with the energy of a chiral soliton and therefore ignored in deriving Eq. (17).

### Appendix C: Fit for $c_v$

We fit the numerical result of the phase boundary between AVL and BVL established in Ref. [73] with the function  $\mu_I = \mu_I^c(\mu_B)$  given in Eq. (17), leading to  $c_v = 1.06$ . The region with larger  $\mu_I/m_\pi$  gives a better fit, because the tension of a neutral pion vortex in Eq. (28) is more negligible for larger  $\mu_I$ .

<sup>7</sup> This is the same as Ref. [64]. It differs from that in Ref. [68] but the asymptotic behavior at large  $\mu_I$  is the same:  $\xi^{-2} \sim \mu_I^2$ .

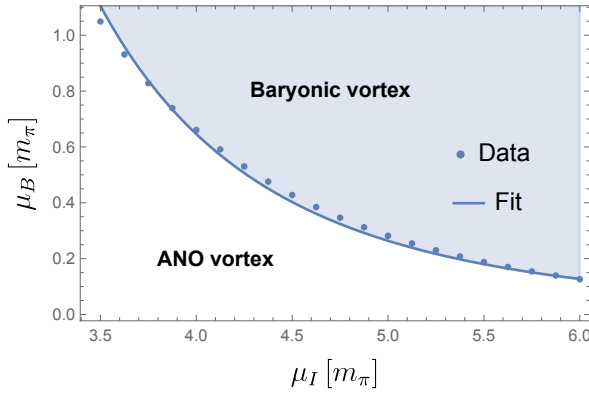


FIG. 3: The fitting for  $c_v$ . Baryonic vortices constitute the BVL while ANO vortices comprise the AVL.

Note that this numerical study is done with  $\mu_I \gtrsim 3.5m_\pi$ . For  $\mu_I \lesssim 3.5m_\pi$ , we found no stable solution within our numerical approach as stated in Ref. [73]. However, that does not rule out the possibility of the existence of solutions. Rigorously speaking, we do not know what happens to the baryonic vortex for  $\mu_I \lesssim 3.5m_\pi$  within  $\mathcal{O}(p^2)$  ChPT.

#### Appendix D: Further details on the phase diagram

We present several scales of  $\mu_I$  and  $B$  given by intersections of curves in the phase diagram Fig. 1. We adopt  $m_\pi = 139$  MeV,  $f_\pi = 93$  MeV,  $e \sim 0.303$ . As a reference, we take  $\mu_B = 1$  GeV. For the unit conversion of the magnetic field,  $1 \text{ MeV}^2 \simeq 5.13 \times 10^{13} \text{ G}$ .

First, the intersection of  $\tilde{B}_{\text{CSL}}$  and  $B_*$  reads Eq. (19). The specific value is  $(307 \text{ MeV}, 4.28 \times 10^{17} \text{ G})$ . This is a triple point at which the line  $\mu_I = \mu_I^c$  also ends.

Next, we show the intersections between  $B_{c2}$  and the other phase boundaries:

$$1) \quad B_{c2} = B_{\text{CSL}} \\ \leftrightarrow \mu_I^2 = \frac{8\pi m_\pi f_\pi^2}{\mu_B} + \sqrt{\frac{64\pi^2 m_\pi^2 f_\pi^4}{\mu_B^2} + m_\pi^4}. \quad (29)$$

The intersection is  $(257 \text{ MeV}, 1.02 \times 10^{19} \text{ G})$ .

$$2) \quad B_{c2} = \tilde{B}_{\text{CSL}} \\ \leftrightarrow \mu_I^2 = \sqrt[3]{\frac{8\pi m_\pi^5 f_\pi^2}{\mu_B} + \sqrt{\Delta}} + \sqrt[3]{\frac{8\pi m_\pi^5 f_\pi^2}{\mu_B} - \sqrt{\Delta}} \\ \Delta \equiv \frac{64\pi^2 m_\pi^{10} f_\pi^4}{\mu_B^2} - \frac{m_\pi^{12}}{27}. \quad (30)$$

The intersection is  $(181 \text{ MeV}, 3.59 \times 10^{18} \text{ G})$ .

$$3) \quad B_{c2} = B_*(\mu_I \rightarrow \infty) = c_b \pi e f_\pi^2 \\ \leftrightarrow \mu_I^2 = \frac{1}{2} \left( c_b \pi e f_\pi^2 + \sqrt{c_b^2 \pi^2 e^2 f_\pi^4 + 4m_\pi^4} \right). \quad (31)$$

The virtual intersection is  $(145 \text{ MeV}, 4.46 \times 10^{17} \text{ G})$ . Typical scale of BVL magnetic field can be estimated by such asymptotic  $B_*(\mu_I \rightarrow \infty) = c_b \pi e f_\pi^2$ . The extension in the backward direction (towards smaller  $\mu_I$ ) of such a horizontal line  $B = B_*(\mu_I \rightarrow \infty)$  has the (virtual) intersection with the  $B_{c2}$  shown above.

Also,  $B_*$  intersects with  $B_{c1}$  at

$$B_{c1} = B_* \leftrightarrow \mu_I = e f_\pi \exp(4\pi c_b) \sim 17 \text{ TeV}, \quad (32)$$

which is quite large and out of the range of ChPT.

Eventually, we discuss phase diagrams at extreme values of  $\mu_B$ , as shown in Fig. 4. In the limit  $\mu_B \rightarrow \infty$ , the fact  $\mu_I^c \rightarrow m_\pi$  implies that the only possible vortex lattice for  $B < B_*$  is the BVL. The transition between the BVL and the CSL-AVL intersection becomes essentially controlled by the lattice density. Meanwhile, the phase without vortices is dominated by the CSL when  $B > B_{c2}$  and by the uniform CPC when  $B < B_{c1}$ . All ground states except CPC carry a baryon number. On the contrary, for  $\mu_B \rightarrow 0$ , the infinite  $\mu_I^c \rightarrow \infty$  means that BVL cannot emerge. Actually, there is no involvement of  $\pi^0$ , so the vortex phase is purely the AVL that satisfies  $B_{c1} < B < B_{c2}$  with  $B = B_*$  prescribing only a crossover (not a phase transition). The region with  $B < B_{c1}$  remains the uniform CPC. No state carries a baryon number in this limit.

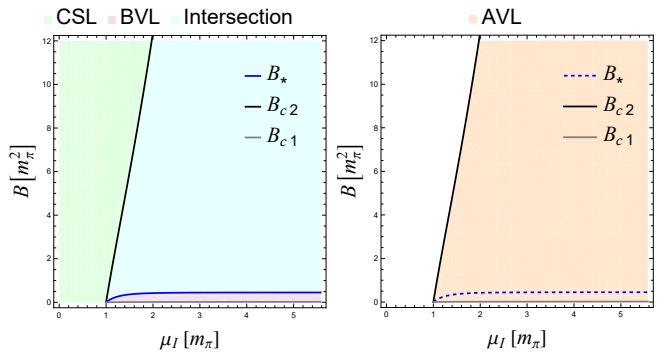


FIG. 4: Phase diagrams at  $\mu_B \rightarrow \infty$  (left) and  $\mu_B = 0$  (right).